Journal of Solid State Chemistry **155,** 359–365 (2000)
doi:10.1006/jssc.2000.8925, available online at http://www.idealibrary.com on IDEAL®

An Electron Diffraction and Crystal Chemical Investigation of Oxygen/Fluorine Ordering in Rutile-Type Iron Oxyfluoride, FeOF

Frank J. Brink,*,† Ray L. Withers,*,[1] and John G. Thompson*

*Research School of Chemistry, Australian National University, Canberra, ACT 0200, Australia; and †Electron Microscope Unit, Research School of Biological Sciences, Australian National University, Canberra, ACT 0200, Australia

Received June 26, 2000; accepted August 9, 2000; published online November 29, 2000

Rutile-type iron oxyfluoride, FeOF, has been synthesized by the reaction of FeF_3 with Fe_2O_3 in a sealed platinum tube at 950°C. The compound was previously believed to have a random distribution of oxygen and fluorine anions surrounding each of the Fe^{3+} cations. In this work, electron diffraction experiments have revealed the presence of a characteristic diffuse intensity distribution in the form of continuous rods of diffuse intensity running along both the [110]* and [1$\bar{1}$0]* directions of reciprocal space through the $(h+k+l)$ = odd parent rutile reflections. Fe^{3+} shifts induced by local O/F ordering are shown to be responsible for the characteristic reciprocal space intensity distribution of this observed diffuse scattering. The continuous $\langle 110 \rangle$* rods of diffuse intensity require the existence of orthogonal {110} planes within the parent rutile structure which exhibit long-range, two-dimensional, oxygen/fluorine ordering, but with no correlation from one {110} plane to the next. A crystal chemical explanation is proposed to support this argument. © 2000 Academic Press

INTRODUCTION

Oxyfluoride compounds form a natural bridge between the oxide and fluoride families of compounds and research into them has been steadily on the increase over many years (1–4). To date, most oxyfluorides have been reported to exhibit random anion site disorder. This apparent absence of oxygen–fluorine ordering is usually attributed to the rather similar ionic sizes of O^{2-} and F^- ions. On the other hand, the strong electronegativity difference between oxygen and fluorine should provide a strong driving force for ordering, particularly for compounds with simple composition ratios (2). Perhaps the most simple such formulation known corresponds to the $M^{3+}OF$ (M = Fe, Ti, V, ...,) transition metal oxyfluorides (2, 5–9) which crystallize in the rutile structure type (see Fig. 1), apparently with no oxygen–fluorine ordering.

[1] To whom all correspondence should be addressed.

The FeOF transition metal oxyfluoride was first prepared by Hagenmuller *et al.* (5) and was found to possess a rutile-type structure with cell parameters $a = 4.647(5)$ Å and $c = 3.048(9)$ Å. The possibility of oxygen–fluorine ordering therein was first raised by Chappert and Portier (6, 7) as a result of their Mössbauer studies that indicated a single unique environment for the Fe^{3+} cation. They concluded that there must be some sort of ordered distribution of oxygen and fluorine ions leading to a superstructure of a rutile-type parent structure that is difficult to observe with either X-ray or neutron diffraction. Vlasse *et al.* (10) followed this latter suggestion up with a precise single crystal X-ray diffraction experiment. No evidence, however, was found for any such superstructure or for any oxygen–fluorine ordering.

Given the similarity of the atomic scattering factors of O and F for all three commonly used radiations (X-ray, neutrons, and electrons) (3) and their weakness relative to the atomic scattering factor of Fe, it is clear that any diffraction evidence for O/F ordering is always going to be weak in intensity relative to the average structure Bragg reflections and difficult to detect. In this study we therefore focus on electron diffraction which has a proven ability to detect weak features of reciprocal space often undetected by X-ray or neutron diffraction.

SYNTHESIS AND DATA COLLECTION

The FeOF transition metal oxyfluoride is difficult to synthesize in pure single phase form via the action of FeF_3 on α-Fe_2O_3 as a result of the unavoidable presence of some water associated with the FeF_3 starting material (5–9). An additional problem is the volatility of the FeF_3 starting material necessitating the use of sealed Pt tubes.

The FeOF used in this study was prepared by the reaction of a 1:1.12 molar ratio of α-Fe_2O_3 (Halewood Chem. Ltd., 99.999%) and FeF_3 (Cerac, 99.5%, nominally anhydrous) at 950°C in a sealed platinum tube for 24 h. The reactants were manipulated in an argon-filled dry box to avoid

0022-4596/00 $35.00

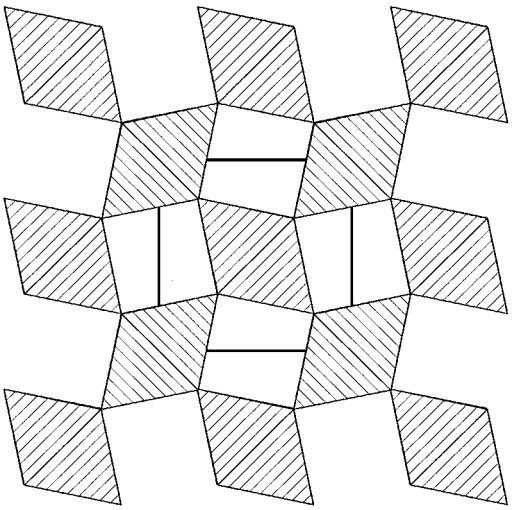

FIG. 1. Schematic [001] projection of the FeOF rutile-type average structure. The FeA_6 (A = anion) octahedra are shown hatched. The unit cell is outlined.

contamination with air or water vapor. Initial experiments, using equimolar amounts (5–9) of the starting materials always resulted in traces of Fe_2O_3 in addition to the desired FeOF in the resultant reaction mixture. Subsequent analysis of the FeF_3 starting material by FTIR invariably indicated the presence of a certain amount of water. Some hydrolysis of the FeF_3 was therefore inevitable during the synthesis resulting in the loss of fluorine in the form of HF gas. As dehydration of hydrated FeF_3 and *ab initio* synthesis of anhydrous FeF_3 (11) both require exotic apparatus (pure iron vessels and tubing) and extreme reaction conditions (HF gas at $>800^\circ$C) not available to us, commercially available material had to be used. By adding a relatively small (0.12 mol) excess of FeF_3 to the initial starting mixture, however, it was found to be possible to account for the fluorine loss associated with the slightly hydrated FeF_3 starting material and to consistently produce single phase FeOF.

In agreement with the previously reported results of Chappert and Portier (6, 7) and Chamberland *et al.* (8, 9), we find that FeOF cannot be formed below 925°C and, on heating from room temperature, begins to unmix back to Fe_2O_3 and FeF_3 at temperatures above $\sim 635^\circ$C.

XRD data collected from a Guinier–Hägg camera ($\lambda = 1.5406$ Å), using an internal Si (NBS No. 640) standard, were used to refine the unit cell parameters ($a = 4.6431(7)$ Å, $c = 3.0436(5)$ Å). Samples suitable for transmission electron microscope (TEM) work were prepared by the dispersion of finely ground material onto a holey carbon film. Electron diffraction patterns (EDPs) were obtained using Philips 430, JEOL 2000FX, and JEOL 100CX TEMs.

ELECTRON DIFFRACTION RESULTS

Initial investigation of reciprocal space revealed a confusing mix of diffraction features in addition to the strong sharp Bragg reflections of the underlying rutile-type average structure (hereafter labeled **G**) (see Figs. 2–5). In some EDPs, virtually continuous lines of diffuse intensity were observed, particularly for zone axis orientations relatively close to [001] (see, for example, Figs. 2a and 2b) while, in others, apparently sharp superlattice reflections were visible (see Figs. 3a and 3b).

Figure 2a, for example, shows typical ⟨014⟩ and (b) ⟨013⟩ zone axis microdiffraction patterns, representative of orientations close to the [001] zone axis orientation. In addition to the sharp rutile-type parent reflections, strong

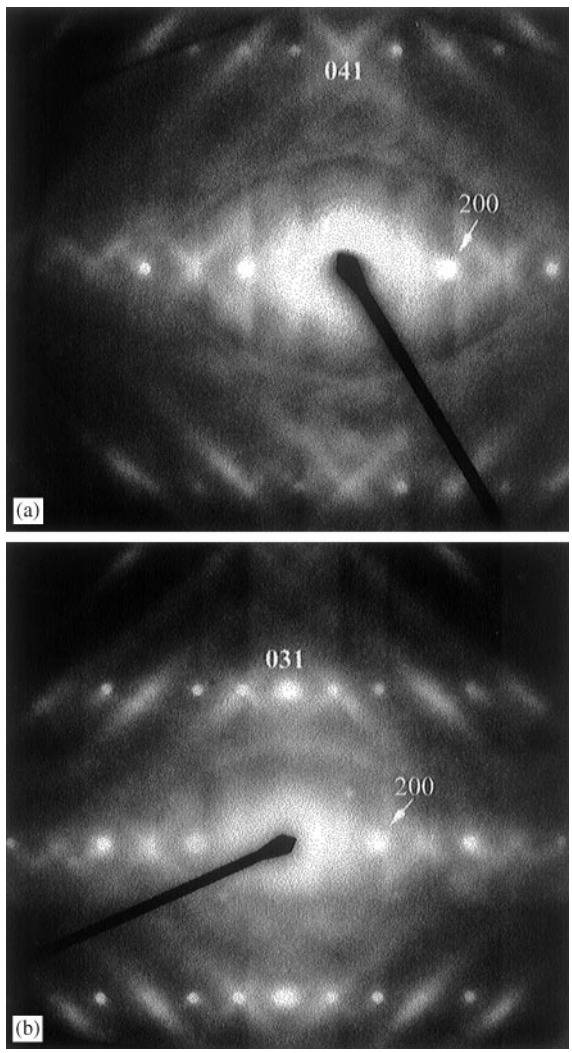

FIG. 2. Typical (a) ⟨014⟩ and (b) ⟨013⟩ zone axis microdiffraction EDPs of FeOF. Note the characteristic diffuse streaking in both and the fact that this diffuse streaking only runs through rutile parent reflections for which $(h + k + l)$ is odd.

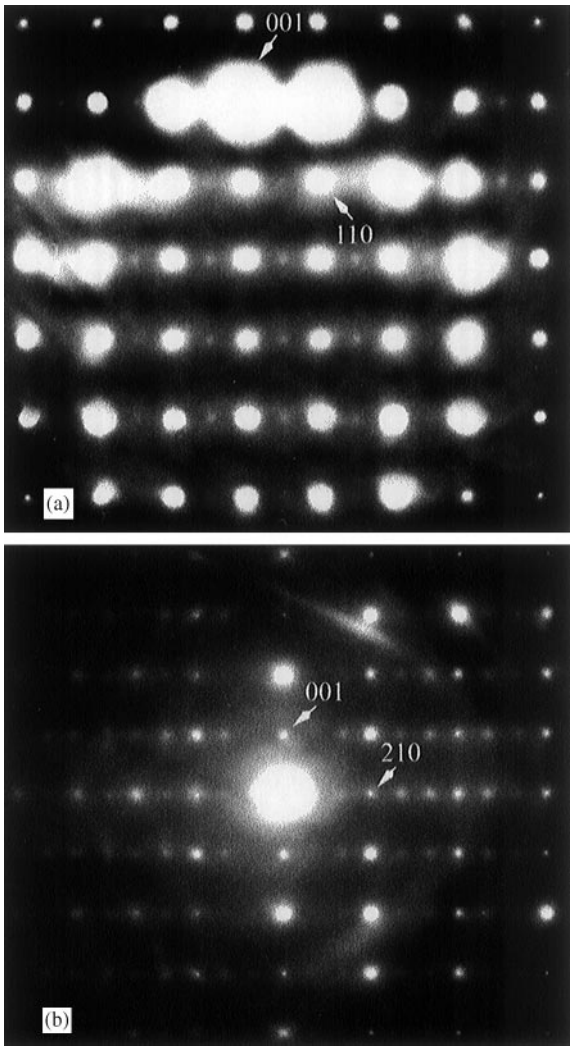

FIG. 3. Selected area EDPs taken close to (a) a ⟨110⟩ zone axis orientation and (b) a ⟨120⟩ zone axis orientation. Rutile-type parent reflections are labeled. Note the presence of additional satellite reflections in both.

(virtually continuous) lines of polarized diffuse intensity are clearly visible running approximately along the [110]* and [1$\bar{1}$0]* directions of reciprocal space. It is also apparent that there is a strong angular, or azimuthal, variation of the intensity of these diffuse streaks, indicating that atomic displacements are making the major contribution toward the observed intensities. The transverse polarized character of the diffuse streaking (i.e., the fact that the intensity of the diffuse streaking is always strongest when looking out along directions of reciprocal space perpendicular to the direction of streaking itself) implies that the associated atomic shifts must also be largely transverse polarized; i.e., the atomic shifts giving rise to the diffuse streaking along [110]* must be largely due to the atomic shifts along [1$\bar{1}$0] and vice versa.

The final important feature to notice about Fig. 2 is that there is clearly an extinction condition operating in that the diffuse streaking does not run through all parent rutile reflections, but only through those for which $(h + k + l)$ is odd (e.g., in Fig. 2a) diffuse streaks run through the 041 reflection but not through the neighboring 141 reflection whereas, in Fig. 2b, diffuse streaks run through the 131 reflection but not the neighboring 031 reflection, etc.). This characteristic extinction condition can be easily obscured at more major zone axis orientations such as [001] itself or ⟨110⟩ and ⟨120⟩ (cf. Figs. 3 and 4) where stronger multiple scattering routes connecting the $(h + k + l) = \text{odd}$ and $(h + k + l) = \text{even}$ reflections exist. This essentially body-centered extinction condition is absolutely characteristic of the diffuse streaking and strongly suggests that atomic displacements of the Fe atoms must be largely responsible (keep in mind that the Fe atoms occupy the origin and the body-centered positions in the rutile-type average structure).

Tilting to zone axis orientations perpendicular to the [001] orientation, as shown in the close to ⟨110⟩ and close to ⟨120⟩ zone axis orientations of Figs. 3 and 4, results in

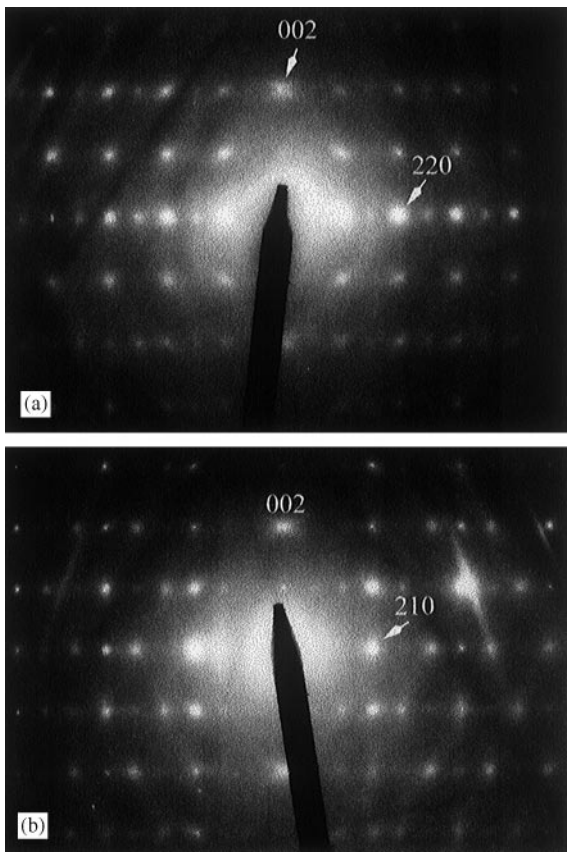

FIG. 4. EDPs similar to those in Fig. 3, but tilted a little further off axis in order to minimize the effects of dynamical diffraction. Note the characteristic extinction conditions now clearly visible.

what appear to be discrete additional "satellite" reflections occurring at reciprocal space positions $\mathbf{G} \pm [m\,n\,0]^*$, where $\mathbf{G} = [hkl]^*$ (h, k, l all integers) and $\pm m + n = 1$. In Fig. 3a, for example, $\mathbf{G} \pm 1/2\langle 110\rangle^*$ type satellite reflections corresponding to $m = 1/2$ and $n = 1/2$ are apparent whereas, in Fig. 3b, $\mathbf{G} \pm 1/3\ \langle 210\rangle^*$ type satellite reflections corresponding to $m = 2/3$ and $n = 1/3$ are clearly visible. Similarly, at $\langle 310\rangle$ zone axis orientations, $\mathbf{G} \pm 1/4[310]^*$ type satellite reflections corresponding to $m = 3/4$ and $n = 1/4$ are visible, etc.

At first glance, it appears that these additional satellite reflections, e.g., the $\mathbf{G} \pm 1/3\ \langle 210\rangle^*$ type satellite reflections, apparent on the right-hand side of Fig. 3b, for example, do not appear to obey any particular extinction condition. Tilting slightly further away from the exact zone axis orientation to minimize the effects of multiple scattering (see Fig. 4b), however, shows that these satellite reflections do indeed obey a characteristic extinction condition (cf. Figs. 4b, and 3b) and one that is entirely compatible with that observed for the $\langle 110\rangle^*$ diffuse streaking. The same is also true for the $\langle 110\rangle$ orientation (cf. Figs. 4a and 3a). The only way in which the observation of these apparently sharp satellite reflections can be reconciled with the more-or-less continuous diffuse streaking apparent in EDPs close to [001] is in terms of essentially continuous rods of diffuse intensity along both the [110]* and $[1\bar{1}0]^*$ directions of reciprocal space running through the $(h + k + l) =$ odd parent rutile reflections.

This interpretation may be confirmed by considering an intermediate orientation such as, for example, the $[1\bar{3}5]$ zone axis shown in Fig. 5. Now, in addition to the strong Bragg reflections of the underlying rutile-type parent structure, there exist diffuse dashes (or streaks of rather short duration in reciprocal space). This is exactly as would be expected given that we are now intersecting linear rods of diffuse intensity at an oblique angle. Furthermore, the orientation, location, and intensity distribution of the diffuse dashes in Fig. 5 are also as would be expected given the above description.

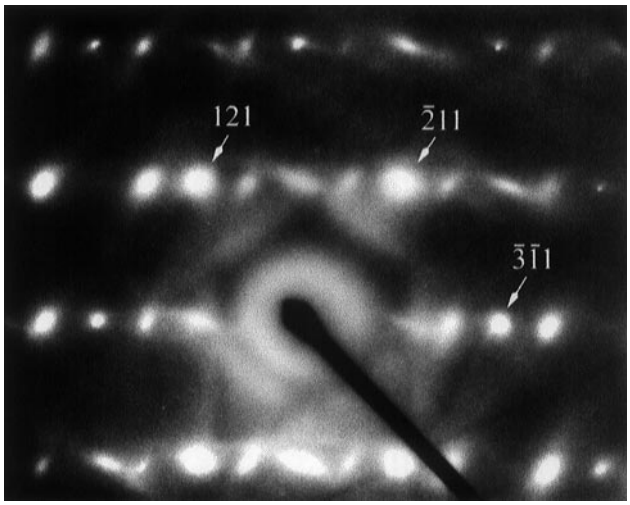

FIG. 5. An intermediate $[1\bar{3}5]$ zone axis EDP. In addition to the labeled rutile-type parent reflections, note the presence of diffuse dashes of limited length consistent with an oblique section of a rod in reciprocal space.

INTERPRETATION

Having established that the reciprocal lattice of FeOF is characterized by continuous, transverse polarized rods of diffuse intensity running along both the [110]* and $[1\bar{1}0]^*$ directions of reciprocal space through the $(h + k + l)$ odd reflections of the rutile-type average structure, the question now becomes what is the crystal chemical origin of this characteristic diffuse distribution?

It is well known that a one-dimensional rod of diffuse intensity running along the [110]* direction of reciprocal space implies the existence of (110) planes of atoms whose displacements and occupancies must be correlated within the plane but totally uncorrelated from plane to plane along the orthogonal [110] direction. (The equivalent statement must also be true for the symmetry-equivalent one-dimensional rod of diffuse intensity running along the orthogonal $[1\bar{1}0]$ direction of reciprocal space).

In the case of rutile-type or FeOF, this requires that we must look for an explanation of the observed diffuse distribution in the correlated occupancies and shifts of the atoms within $\{110\}$ planes, as shown in Fig. 6a. Consider, for example, the [110]* rods of reciprocal space. The transverse polarized diffuse streaking in EDPs such as those in Fig. 2 requires that the responsible atomic shifts must be perpendicular to the [110]* rod direction itself, i.e., in the (110) plane. Indeed it implies that a major component of these shifts must be along the orthogonal $[1\bar{1}0]$ direction.

More specifically still, the systematic absence of $\mathbf{G} \pm \varepsilon[110]^*$ streaks in $[1\bar{1}0]$ zone axis EDPs (see Figs. 3a and 4a) requires that the associated displacements must be entirely along the orthogonal $[1\bar{1}0]$ direction of real space. In other words, the rods of diffuse intensity along [110]* are due to atomic displacements along $[1\bar{1}0]$ while the rods of diffuse intensity along $[1\bar{1}0]^*$ are due to atomic displacements along [110]. (Such basal plane shifts of the Fe atoms are also strongly supported by the average structure refinement result of Vlasse *et al.* (10) that the "… thermal vibration ellipsoid observed for the iron atoms is very much flattened perpendicular to the c axis …").

At this point it becomes convenient to consider the observed diffuse distribution from a modulation wave point of view (12–14). Each point on the observed diffuse distribution is thus described as $\mathbf{G} \pm \mathbf{q}$ and the various modulations are treated as independent modulation waves. Furthermore,

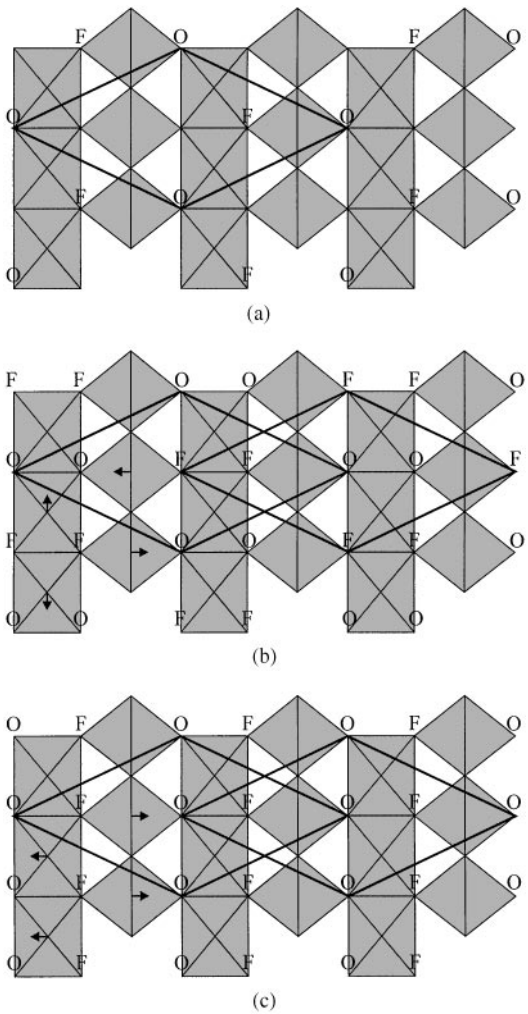

FIG. 6. Schematic representation of the $\langle 110 \rangle$ planes of the rutile-type structure. The first diagram (a) shows the honeycomb generated if opposite corners of each octahedron are constrained to be of opposite type, i.e., if one is O then the other must be F and vice versa. Note that two such honeycomb arrays are required to cover all anion sites in this projection. The two possible fully ordered arrangements are shown in (b) and (c). Note the relationship between the resulting "supercells" in each case.

the modulation wave-vectors are broken into two classes, those along [110]* and those along $[1\bar{1}0]$*. The former are written in the generic form $\mathbf{q}_1 = \varepsilon[110]$* and the latter in the form $\mathbf{q}_2 = \varepsilon[1\bar{1}0]$*, where it is implicitly understood that ε can run over the range from 0 to 1/2.

As discussed above, the body-centered tetragonal nature of the sublattice formed by the Fe atoms in FeOF (see Fig. 1) combined with the observed extinction condition observed for the diffuse, i.e., $F(\mathbf{G} \pm \mathbf{q}_1, \mathbf{q}_2) = 0$ unless $(h + k + l)$ is odd, implies not only that shifts on the Fe atoms must be primarily responsible for the observed diffuse distribution but also that the Fe atom shifts of the two independent Fe atoms per parent unit cell must be anticorrelated, i.e., have the opposite sign.

Consider, for example, the displacive contribution of the Fe atoms to the structure factor at the reciprocal space position $(\mathbf{G} + \mathbf{q}_2)$. Following (12), this is given by

$$F_{\text{disp}}(\mathbf{G} + \mathbf{q}_2) \propto \sum_{\mu} f_{\mu}^{\text{av}} \exp\{2\pi i\, \mathbf{G} \cdot \mathbf{r}_{\mu}\}$$
$$2\pi(\mathbf{G} + \mathbf{q}_2) \cdot \mathbf{e}_{\mu}(\mathbf{q}_2) \cdots \qquad [1]$$

Here $\mathbf{r}_{\mu}$ labels the position of the μth independent Fe atom per parent unit cell and $\mathbf{e}_{\mu}(\mathbf{q}_2)$ represents the displacement eigenvector (or shift of this atom) associated with the $\mathbf{q}_2$th modulation wave-vector.

Now within each $(1\bar{1}0)$ plane of atoms (see Figs. 1 and 6) there exist two independent Fe atoms per parent unit cell, Fe_1 at (0, 0, 0) and Fe_2 at (1/2, 1/2, 1/2), which will contribute to the structure factor at $(\mathbf{G} + \mathbf{q}_2)$. The observed extinction condition, $F(\mathbf{G} \pm \mathbf{q}_1, \mathbf{q}_2) = 0$ unless $(h + k + l)$ is odd, requires that $\mathbf{e}_{\text{Fe}2}(\mathbf{q}_2) = -\mathbf{e}_{\text{Fe}1}(\mathbf{q}_2)$ as can be seen by substitution into Eq. [1] above, giving

$$F_{\text{disp}}(\mathbf{G} + \mathbf{q}_2) \propto 2\pi(\mathbf{G} + \mathbf{q}_2) \cdot \mathbf{e}_{\text{Fe}1}$$
$$+ 2\pi(\mathbf{G} + \mathbf{q}_2) \cdot \mathbf{e}_{\text{Fe}2} \exp\{\pi i(h + k + l)\}$$
$$= [2\pi(\mathbf{G} + \mathbf{q}_2) \cdot \mathbf{e}_{\text{Fe}1}][1 - \exp\{i\,\pi(h + k + l)\}],$$

which $= 0$ unless $(h + k + l)$ is odd as experimentally observed.

While these $\langle 110 \rangle$ displacive shifts of the Fe atoms could in principle arise without an underlying compositional cause, it seems far more likely that the Fe shifts are a response to oxygen/fluorine ordering within each $\{110\}$ plane.

CRYSTAL CHEMICAL CONSIDERATIONS

The question now becomes what sort of oxygen/fluorine ordering could be responsible for these $\langle 110 \rangle$ Fe shifts. The crystal chemical reasons for the Fe shifts can be understood from a bond length–bond valence analysis (15) of the average structure of FeOF using the refined fractional coordinates of Vlasse *et al.* (10). The apparent valence (AV) of a particular ion is defined as the bond valence sum arising from the surrounding ions of opposite charge (15). Such apparent valence calculations indicate that oxygen, with a calculated AV of 1.556, is significantly underbonded in the average structure anion position while fluorine (AV = 1.223) is significantly overbonded (see Table 1). Using the R_0 parameters of Brese and O'Keeffe (15), the ideal anion–Fe^{3+} separation distance when the anion is O^{2-} would be 1.909 Å while the ideal anion–Fe^{3+} separation distance when the anion is F^- would be 2.076 Å. The experimental average anion–Fe^{3+} separation distance reported by Vlasse *et al.* (10) is, not surprisingly, halfway in between at 2.00 Å.

TABLE 1
Bond Valence Sums (AVs) for the Refined Average Structure of FeOF (10, 15)

Atom	AV	Expected AV
Fe (assuming anions all F)	2.78	3.00
Fe (assuming anions all O)	3.11	3.00
O	1.56	2.00
F	1.22	1.00

Crystal chemically this implies that O^{2-} ions will attract neighboring Fe^{3+} cations while F^- ions will repel them. If we consider any particular (110) plane of ions (see Fig. 6a), it seems logical to suggest that opposite corners of each FeA_6 octahedraon (A for anion) should necessarily be of opposite type, i.e., if one corner is fluorine then the other should be oxygen and vice versa (see Fig. 6a). This would then allow the iron atom to shift out of the center of the octahedra toward the oxygen ions and away from the fluorine ions as desired. It would also imply, in agreement with the original Mössbauer results of Chappert and Portier (6) that each Fe^{3+} cation is in a unique environment surrounded always by $3O^{2-}$ ions and $3F^-$ ions.

The application of such a rule within a $\{110\}$ plane, starting at an arbitrary apex of any one octahedron, generates an ordered honeycomb array of oxygen and fluorine ions, with an in-plane superlattice unit cell as shown in Fig. 6a. Notice that there are two such honeycomb arrays, at this stage still allowed to be independent of each other. The requirement that opposite vertices of each octahedron should be of opposite type does not, of itself, determine the phase relationship between these two honeycomb arrays. Moreover, a single ordered honeycomb array would not of itself force Fe cations to displace solely along $\langle 110 \rangle$ directions. It is therefore necessary to consider the possible phase relationships between the two honeycomb arrays.

Matching anions of the same type (i.e., O–O, F–F) across the short edge of the octahedra leads to the ordering pattern shown in Fig. 6b. Note that in this case there is a "phase" reversal of 180° between the two honeycomb arrays for a parent rutile translation of [110]. Note furthermore that such an ordering pattern would constrain half the Fe cations to displace along the parent c direction with the other half constrained to displace along the orthogonal $\langle 110 \rangle$ parent direction (see Fig. 6b). This is not compatible with experimental observation as discussed above. The alternative fully ordered possibility, matching anions of the opposite type, (i.e., O–F, F–O) across the short edge of the octahedra, gives rise to the ordering pattern shown in Fig. 6c. This time, the two honeycomb arrays are in "phase" for a parent rutile translation of [110]. Furthermore, all Fe cations are constrained to shift solely along $\langle 110 \rangle$ parent rutile directions while $\mathbf{e}_{Fe2}$ is necessarily of opposite sign to $\mathbf{e}_{Fe1}$, just as required experimentally. There is, theoretically, a third alternative possibility whereby the two honeycomb arrays are not correlated. This, however, would give rise to additional diffuse rods at positions of reciprocal space which are not observed experimentally.

We therefore believe that oxygen and fluorine ions are in essence completely ordered within any one $\{110\}$ type plane with the O/F ordering pattern as shown in Fig. 6c. The observed $\langle 110 \rangle^*$ rods of diffuse intensity, however, require that there is no correlation in this ordering pattern from one such $\{110\}$ plane to the next. Comparison of Fig. 1 with Fig. 6c shows that this should not be unexpected. Indeed there would appear to be absolutely no crystal chemical reason at all for any such correlation to exist. A possible crystal chemical explanation as to why anions of the opposite type (i.e., O–F, F–O) should necessarily be matched across the short edge of the octahedra can be found in the 2.609-Å separation across the short edge of the octahedra. Consideration of nonbonded anion–anion interaction energies (16) suggests a minimum for anions of the opposite type (i.e., O–F, F–O) at either end of this short 2.609-Å separation distance.

CONCLUSION

The final point that has been arrived at is that there is no contradiction at all between the original Mössbauer results (requiring that each Fe atom be in a unique environment) and diffraction results, but only if the assumption of three-dimensional long-range order is thrown away and the observed diffuse scattering (in the form of $\langle 110 \rangle^*$ rods of diffuse intensity running through the $(h + k + l)$ odd rutile parent reflections) taken into account. It is the (completely understandable from the crystal chemical point of view) lack of correlation from one fully O/F ordered $\{110\}$ plane to the next along the orthogonal $\langle 110 \rangle$ direction that is responsible for the observed diffuse distribution and that prevents the condensation of a long-range (O/F) ordered (from the conventional crystallographic point of view) superstructure phase.

Careful consideration shows that there are only four distinct local O_3F_3 ordering patterns possible for any one particular FeO_3F_3 octahedra that will give rise to a resultant displacement of the Fe atom (away from the octahedral center) along either the $\pm a$ or $\pm b$ directions. The magnitude of this shift (essentially away from the local F_3 octahedral face and toward the opposite O_3 octahedral face) should be ~ 0.12–0.13 Å in order to satisfy local bond valence requirements (see Table 1). By analogy, one might expect similar behavior for all isomorphous M^{3+} OF (M = Ti, V, Al, …) oxyfluorides (5–9).

Furthermore, it may well be the case that the local crystal chemistry of a range of other oxyfluoride systems (many of

which spectroscopic and bond valence considerations suggest should also be locally ordered (3)) cannot be properly understood until diffuse distributions of the type reported in the present paper are observed and properly taken into account.

REFERENCES

1. J. Ravez, *J. Phys. III Fr.* **7,** 1129–1144 (1997).
2. P. Hagenmuller, *in* "Perspectives in Solid State Chemistry" (K. J. Rao, Ed), pp. 66–78, Narosa, New Delhi, 1995.
3. L.-S. Du, F. Wang, and C. P. Grey, *J. Solid State Chem.* **140,** 285–294 (1998).
4. T. Vogt, P. M. Woodward, B. A. Hunter, A. K. Prodjosantoso, and B. J. Kennedy, *J. Solid State Chem.* **144,** 228–231 (1999).
5. P. Hagenmuller, J. Portier, J. Cadiou, and R. DePape, *C. R. Acad. Sci.* **260,** 4768 (1965).
6. J. Chappert and J. Portier, *Solid State Commun.* **4,** 185 (1996).
7. J. Chappert and J. Portier, *Solid State Commun.* **4,** 395 (1966).
8. B. L. Chamberland and A. W. Sleight, *Solid State Commun.* **5,** 765–767 (1967).
9. B. L. Chamberland, A. W. Sleight, and W. H. Cloud, *J. Solid State Chem.* **2,** 49–54 (1970).
10. M. Vlasse, J. Massies, and G. Demazeau, *J. Solid State Chem.* **8,** 109 (1973).
11. W. Kwasnik, *in* "Handbook of Preparative Inorganic Chemistry" (G. Brauer, Ed), 2nd ed., Vol. I, p. 226, Academic Press, New York, 1963.
12. R. L. Withers, S. Schmid, and J. G. Thompson, *Prog. Solid State Chem.* **26,** 1 (1998).
13. T. R. Welberry and R. L. Withers, *J. Appl. Crystallogr.* **23,** 303 (1990).
14. B. D. Butler, R. L. Withers, and T. R. Welberry, *Acta Crystallogr. A* **48,** 737 (1992).
15. N. E. Brese and M. O'Keeffe, *Acta Crystallogr. B* **47,** 192 (1991).
16. M. O'Keeffe and B. G. Hyde, *in* "Structure and Bonding in Crystals" (M. O'Keeffe and A. Navtotsky, Eds.), Vol. I, Chap. 10, pp. 66–78, Academic Press, New York, 1981.